

Evolution of light trapped by a soliton in a microstructured fiber

S. Hill, C. E. Kuklewicz, U. Leonhardt, F. König

School of Physics and Astronomy, University of St Andrews, North Haugh, St Andrews, Fife, KY16 9SS, UK.

fewk@st-andrews.ac.uk

<http://www.st-andrews.ac.uk/qinfo/>

Abstract: We observe the dynamics of pulse trapping in a microstructured fiber. Few-cycle pulses create a system of two pulses: a Raman shifting soliton traps a pulse in the normal dispersion regime. When the soliton approaches a wavelength of zero group velocity dispersion the Raman shifting abruptly terminates and the trapped pulse is released. In particular, the trap is less than 4 ps long and contains a 1 ps pulse. After being released, this pulse asymmetrically expands to more than 10 ps. Additionally, there is no disturbance of the trapping dynamics at high input pulse energies as the supercontinuum develops further.

© 2021 Optical Society of America

OCIS codes: (060.7140) Ultrafast processes in fibers; (190.5530) Pulse propagation and temporal solitons; (190.4370) Nonlinear optics, fibers

References and links

1. J. M. Dudley, G. Genty, S. Coen, "Supercontinuum Generation in Photonic Crystal Fiber," *Rev. Mod. Phys.* **78**, 1135–1184 (2006).
2. N. Ishii, C. Y. Teisset, S. Kohler, E. E. Serebryannikov, T. Fuji, T. Metzger, F. Krausz, A. Baltuska, A. M. Zheltikov, "Widely Tunable Soliton Frequency Shifting of Few-Cycle Laser Pulses," *Phys. Rev. E* **74**, 036617 (2006).
3. E. E. Serebryannikov, A. M. Zheltikov, N. Ishii, C. Y. Teisset, S. Kohler, T. Fuji, T. Metzger, F. Krausz, A. Baltuska, "Soliton Self-Frequency Shift of 6-fs Pulses in Photonic-Crystal Fibers," *Appl. Phys. B* **81**, 585–588 (2005).
4. P. Falk, M. H. Frosz, O. Bang, L. Thrane, P. E. Andersen, A. O. Bjarklev, K. P. Hansen, and J. Broeng, "Broadband light generation at ~ 1300 nm through spectrally recoiled solitons and dispersive wave," *Opt. Lett.* **33**, 621–623 (2008).
5. N. Nishizawa and T. Goto, "Characteristics of pulse trapping by use of ultrashort soliton pulses in optical fibers across the zero-dispersion wavelength," *Opt. Express* **10**, 1151–1159 (2002).
6. N. Nishizawa, T. Goto "Pulse Trapping by Ultrashort Soliton Pulses in Optical Fibers Across Zero-Dispersion Wavelength," *Opt. Lett.* **27**, 152–154 (2002).
7. N. Nishizawa, T. Goto "Ultrafast All Optical Switching by Use of Pulse Trapping Across Zero-Dispersion Wavelength," *Opt. Express* **11**, 359–365 (2003).
8. A. V. Gorbach, D. V. Skryabin "Light Trapping in Gravity-Like Potentials and Expansion of Supercontinuum Spectra in Photonic-Crystal Fibres," *Nature Photonics* **1**, 653–656 (2007).
9. J. C. Travers, A. B. Rulkov, B. A. Cumberland, S. V. Popov, and J. R. Taylor "Visible supercontinuum generation in photonic crystal fibers with a 400 W continuous wave fiber laser," *Opt. Express* **16**, 14435–14447 (2008).
10. B. A. Cumberland, J. C. Travers, S. V. Popov, and J. R. Taylor "Toward visible cw-pumped supercontinua," *Opt. Lett.* **33**, 2122–2124 (2008).
11. A. V. Husakou and J. Herrmann, "Supercontinuum generation of higher-order solitons by fission in photonic crystal fibers," *Phys. Rev. Lett.* **87**, 203901 (2001).
12. G. P. Agrawal, *Nonlinear Fiber Optics* (Academic Press, 2006).
13. T. G. Philbin, C. Kuklewicz, S. Robertson, S. Hill, F. König, U. Leonhardt, "Fiber-Optical Analog of The Event Horizon," *Science* **319**, 1367–1370 (2008).

14. L. Gagnon, P. A. Bélanger, “Soliton Self-Frequency Shift Versus Galilean-Like Symmetry,” *Opt. Lett.* **15**, 466–468 (1990).
 15. Measured data provided by Crystal Fibre A/S, Denmark.
 16. F. X. Kärtner, *Few-Cycle Laser Pulse Generation and Its Applications: Vol 95* (Springer, 2004).
 17. J. M. Dudley, L. Provino, N. Grossard, H. Mailotte, R. S. Windeler, B. J. Eggleton, S. Coen “Supercontinuum generation in air-silica microstructured fibers with nanosecond and femtosecond pulse pumping,” *J. Opt. Soc. Am. B* **19**, 765–771 (2002).
 18. J. Herrmann, U. Griebner, N. Zhavoronkov, A. Husakou, D. Nickel, J. C. Knight, W. J. Wadsworth, P. St. J. Russell and G. Korn, “Experimental Evidence for Supercontinuum Generation by Fission of Higher-Order Solitons in Photonic Fibers,” *Phys. Rev. Lett.* **88**, 173901 (2002).
 19. K. M. Hilligsøe, T. V. Andersen, H. N. Paulsen, C. K. Nielsen, K. Mølmer, S. Keiding, R. Kristiansen, K. P. Hansen, and J. J. Larson, “Supercontinuum generation in a photonic crystal fiber with two zero dispersion wavelengths,” *Opt. Express* **12**, 1045–1054 (2004).
 20. G. Genty, M. Lehtonen, H. Ludvigsen, and M. Kaivola “Enhanced bandwidth of supercontinuum generated in microstructured fibers,” *Opt. Express* **12**, 3471–3480 (2004).
 21. M. H. Frosz, P. Falk, and O. Bang “The role of the second zero-dispersion wavelength in generation of supercontinua and bright-bright soliton-pairs across the zero-dispersion wavelength,” *Opt. Express* **13**, 6181–6192 (2005).
 22. C. Cheng, X. Wang, Z. Fang, B. Shen, “Nonlinear copropagation of two optical pulses of different frequencies in photonic crystal fiber,” *Appl. Phys. B* **80**, 291–294 (2005).
 23. D. V. Skryabin, F. Luan, J. C. Knight, P. St. J. Russell, “Soliton Self-Frequency Shift Cancellation in Photonic Crystal Fibers,” *Science* **301**, 1705–1708 (2003).
 24. The applied scaling factor was as follows: Fig. 6 left:3, right:2; Fig. 8 left:3, right:2.
 25. A. V. Yulin, D. V. Skryabin, and P. St. Russell “Four-wave mixing of linear waves and solitons in fibers with higher-order dispersion,” *Opt. Lett.* **29**, 2411–2413 (2004).
 26. M. L. V. Tse, P. Horak, F. Poletti, N. G. R. Broderick, J. H. V. Price, J. R. Hayes, and D. J. Richardson “Supercontinuum generation at 1.06μ m in holey fibers with dispersion flattened profiles,” *Opt. Express* **14**, 4445–4451 (2006).
-

1. Introduction

When a short and intense pulse of light is launched into a microstructured fiber (MF), nonlinear effects can significantly broaden the spectrum to much more than an octave [1]. These supercontinua are used in a variety of applications such as ultrafast optical switching, spectroscopy, optical coherent tomography, optical clocks, etc. Routinely, around 100-fs pulses are used at a wavelength close to a zero-group velocity dispersion wavelength (ZDW) of the fiber. Using nearly octave-spanning input pulses [2, 3, 4], the phenomenon of ‘pulse trapping’ [5, 6, 7, 8, 9, 10] can be observed. In this effect a non-dispersing pulse can form at the short wavelength end of the broad spectrum. This is surprising because the pulse exists in a region of normal dispersion in the fiber, where the dispersion-induced chirp cannot be cancelled by self-phase modulation. The non-dispersing pulse is trapped behind a fundamental soliton in the anomalous dispersion regime that was generated by soliton fission. Soliton fission can create multiple fundamental solitons, which shift to longer wavelengths via the soliton self-frequency shift (SSFS) [11].

Nishizawa and Goto [6] were the first to demonstrate that a soliton undergoing the SSFS can trap light behind it. The trapped light adjusts to a wavelength that is group velocity matched to the soliton. Because it is forced to travel with the soliton and lies in the normal dispersion regime, it has to shift to shorter wavelengths in order to keep the same group-velocity as the soliton. Gorbach and Skryabin provided an alternative view of pulse trapping [8]: the light is trapped because the soliton accelerates. In simulations they turned off the (negative) acceleration induced by the SSFS and the trapping ceased. The acceleration of the soliton provides a ‘gravity-like’ potential to the trapped pulse.

In this paper we study experimentally the phenomenon of pulse trapping in a fiber with two ZDWs. We use intense few-cycle pulses to generate a soliton and a trapped pulse and focus in particular on the trap dynamics as the soliton reaches the longer zero-dispersion wavelength and

decays. We observe how the light escapes the trap, expanding to a few times the trap length. For higher input pulse energies, a further component in the spectrum at even shorter wavelengths is formed, which dominates the blue end of the evolving supercontinuum.

2. Pulse Trapping

As previously shown, pulse trapping can be explained by an effective potential that is produced by an accelerating pulse – the fundamental soliton undergoing SSFS [8]. The discussion below follows this analysis. The soliton induces a nonlinear modification of the refractive index, n , via the optical Kerr effect [12]:

$$n(I, \omega) = n_0(\omega) + n_2 I, \quad (1)$$

where I is the intensity and n_2 the nonlinear index coefficient, assuming an instantaneous response, and n_0 is the linear index.

Any light field A in the fiber that interacts with the soliton sees the nonlinear contribution to the refractive index, $n_2 I = n - n_0$, and experiences cross-phase modulation (XPM) [13]. The evolution of the slowly varying envelope $A(z, t)$ of this light is governed by [12]:

$$\frac{\partial A}{\partial z} + \beta_1 \frac{\partial A}{\partial t} + \frac{i\beta_2}{2} \frac{\partial^2 A}{\partial t^2} = iVA. \quad (2)$$

z and t are space and time in the laboratory frame. β_1 and β_2 are the dispersion parameters, where $\beta_n = \frac{\partial^n n}{\partial \omega^n} \left(\frac{n(\omega)\omega}{c} \right)$ evaluated at the frequency of A . Since this frequency lies in the normal dispersion regime, β_2 is positive. iVA is the XPM-term and $V(z, t) = 2\gamma|A_s(z, t)|^2$, where A_s is the envelope of the soliton and γ is the nonlinear parameter.

In the co-moving frame given by $T = t - \beta_1 z$ and $Z = z$, eqn. (2) is transformed into the nonlinear Schrödinger equation

$$\frac{\partial A}{\partial Z} + \frac{i\beta_2}{2} \frac{\partial^2 A}{\partial T^2} = iVA. \quad (3)$$

In analogy to the ordinary Schrödinger equation in quantum mechanics, the XPM contribution V induced by the soliton plays the part of a potential barrier.

Equation (3) is transformed into an accelerating frame [8]:

$$\tau = T + \alpha Z^2 / 2 \quad \zeta = Z. \quad (4)$$

Here α describes the rate of the SSFS, which determines the soliton acceleration. For a soliton, $\alpha = -8T_R\beta_{2,s}^2/15T_0^4$ [12]. T_R is the Raman time; the soliton length is T_0 . $\beta_{2,s}$ is the group velocity dispersion at the soliton wavelength, and the minus sign indicates that the accelerating soliton is redshifting and slowing down. The transformation fixes the peak of the accelerating soliton at $\tau = 0$. In this frame, the propagating light A acquires a phase $\phi(\zeta, \tau)$, so $A(Z, T)$ is replaced with $\psi(\zeta, \tau)$ [14]:

$$\psi = Ae^{i\phi} \quad \phi = -\frac{\alpha\zeta\tau}{\beta_2} + \frac{\alpha^2\zeta^3}{6\beta_2}. \quad (5)$$

The propagation equation (3) becomes

$$\frac{\partial \psi}{\partial \zeta} + i\frac{\beta_2}{2} \frac{\partial^2 \psi}{\partial \tau^2} = iU_{\text{eff}}(\tau)\psi, \quad (6)$$

where

$$U_{\text{eff}}(\tau) = (V(\tau) - \alpha\tau/\beta_2). \quad (7)$$

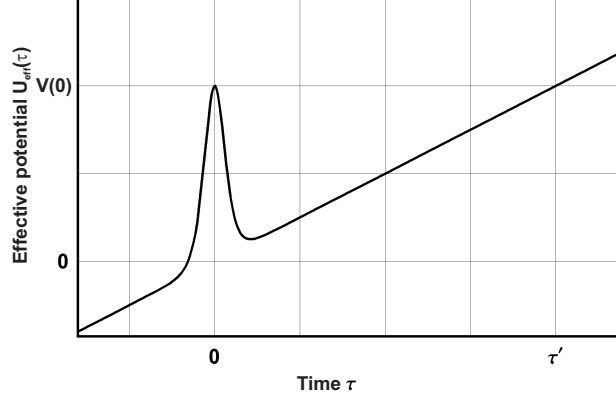


Fig. 1. The potential created by the accelerating soliton. The induced nonlinear index change forms a barrier at $\tau = 0$. The soliton acceleration causes the slope in the potential.

Therefore, in a frame that accelerates with the soliton, other waves propagate in the presence of an effective potential U_{eff} . The first term in equation 7 is the barrier due to XPM and the second term is a linear potential due to the (negative) acceleration α . U_{eff} is sketched in figure 1. The barrier is located at $\tau = 0$ and at $\tau = \tau'$ the linear increase reaches the height of the barrier.

Gorbach and Skryabin pointed out that the potential is ‘gravity-like’, i.e. similar to the gravitational potential on earth. Standing in a lift, the floor acts as a strong potential barrier against the gravitational force. Without gravity, the same potential would be created if the lift had a constant upward acceleration. So a uniformly accelerating barrier can trap objects just as a barrier in a gravitational field does.

As seen in figure 1, the potential can trap light between $\tau = 0$ and $\tau = \tau'$. We can estimate the temporal length of the trap by calculating τ' using $U_{\text{eff}}(\tau') = U_{\text{eff}}(0)$. Approximating $V(\tau') \approx 0$ and inserting α we obtain for an accelerating soliton

$$\tau' = \frac{15T_0^2}{4T_R} \frac{\beta_2}{|\beta_{2,s}|}. \quad (8)$$

τ' depends on the SSFS as well as the ratio of group velocity dispersions for the trapped light and the soliton. In our experiments the trap length is relatively constant, so that the trapped light is expected to have a well defined temporal length. The trap is positioned immediately behind the soliton center at $\tau \geq 0$. In consequence, the trapped light travels at the group velocity of the soliton and slows down with it. The spectrum of the trapped light shifts to a wavelength associated with the same group velocity as the soliton. Accordingly, the potential determines both the spectral and temporal properties of the trapped light.

3. Experiment

To create the trapping soliton as well as the trapped light we couple a few-cycle pulse into a microstructured fiber. We use pulses from a <7 fs Ti:Sapphire laser with a repetition rate of 78 MHz (Rainbow, Femtolasers GmbH). A reflective-optics telescope expands the beam and

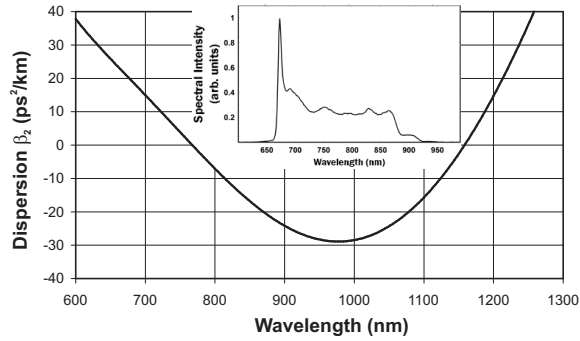


Fig. 2. The group velocity dispersion, β_2 , of the fiber NL-PM-760 [15] and the initial spectrum of the few-cycle pump pulses (inset). The dispersion zeroes at 760 nm and 1160 nm.

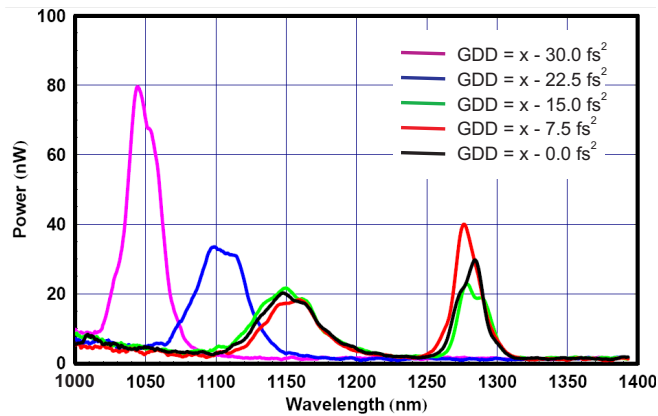


Fig. 3. Output spectra for varying amounts of chirp on the input pulse. The Group-Delay-Dispersion (GDD) before the fiber is varied over 30 fs^2 . The pulse energy is 39 pJ . A GDD of 7.5 fs^2 broadens an unchirped 7-fs pulse by 10% in time.

a parabolic mirror of high numerical aperture focuses the light for fiber coupling. The use of mirrors minimizes dispersion-induced pulse broadening. The 1.8 m-long fiber (NL-PM-760, Crystal Fiber A/S) has zero dispersion at 760 nm and 1160 nm. The dispersion of the fiber and the initial pulse spectrum are shown in figure 2; the nonlinear coefficient is $\gamma = 102(\text{Wkm})^{-1}$ at $\lambda = 780\text{ nm}$ [15]. We rotate the fiber to align the fiber axes to the polarization of the incoming light. As a test of the pulse length at the fiber input face we replaced the fiber with a mirror and backreflected the pulse through the reflective focusing optics. Compensating for group delay dispersion, no significant pulse broadening was observed after the double pass. After the fiber we use a microscope objective to collimate the light and analyze it temporally with an autocorrelator (Pulsecheck, APE GmbH). By tilting the nonlinear crystal of the autocorrelator we perform Frequency-Resolved Optical Gating (FROG) measurements [16]. We also pick off part of our laser output beam, reduce the spectral bandwidth with a 60-nm interference filter, and use it as a reference pulse to record X-FROG traces. The reference pulse was characterized using a FROG measurement to be 35-fs in length (FWHM). Simultaneous to the FROG and X-FROG traces, we measure the spectrum of the trapped light and trapping solitons on a compact CCD-based spectrometer and an optical spectrum analyzer (OSA) for longer wavelengths. Figure 3 demonstrates that the fiber output spectra are very sensitive to the dispersion-induced chirp on the input pulse. In all experiments we adjusted the input chirp to obtain maximum output spectral width (black curve in figure 3).

We create solitons in the near-infrared and trapped light in the visible. Because the input spectrum lies partially in the anomalous dispersion regime beyond 760 nm wavelength, a soliton forms and Raman shifts via the SSFS. The part of the input light that is in the normal dispersion regime and that is trailing the soliton is trapped. In addition there is interaction between light in the two dispersion regimes via self-phase modulation and phasematched amplification of dispersive waves [17, 18, 19, 20, 21]. Therefore, both the trap and trapped light are created by launching a single pulse into the fiber. Since the Raman-shifting soliton traps light, the trapped light has to maintain the soliton group velocity $1/\beta_1(\lambda_s)$ even though the soliton slows down. The trapped light impinges onto the soliton which leads to a blueshift and eventually the maintenance of group velocity matching [13]. Increasing the input pulse energy in the fiber speeds up the SSFS and secondary fundamental solitons are created. For high input pulse energies the primary soliton shifts up to the long ZDW, which it cannot pass. The SSFS abruptly ends and the soliton decays. As the acceleration of the soliton is terminated, the ‘gravity-like’ part of the potential disappears, while the barrier decays slowly, i.e. the trapped light can escape behind the soliton. At the same time the wavelength shift of the trapped light ceases.

3.1. Output Spectra at low pulse energies

When sufficient pulse energy is provided, a soliton is generated and redshifted due to the SSFS. Figure 4 shows that the rate of shifting increases with pulse energy as longer wavelengths are reached within our finite fiber length. Below a wavelength of 700 nm a trapped pulse is created that frequency shifts with the soliton, but in opposite direction. The relative rate of shifting is determined by group velocity matching. Some of the initial pulse energy remains between 700 nm and 900 nm and propagates ahead of the slowing soliton. Note the feature near 1300 nm, which indicates the onset of ‘Cherenkov’ radiation, as discussed in the next section. Similar spectra have been observed in other experiments, see for example [3, 4].

3.2. Output spectra at higher pulse energies

Spectra for higher pulse energies are shown in figure 5. The SSFS has ceased and the soliton has reached a final wavelength of 1150 nm, just below the ZDW of 1160 nm. Approaching this wavelength, the soliton produces dispersive Cherenkov waves around 1300 nm. The production

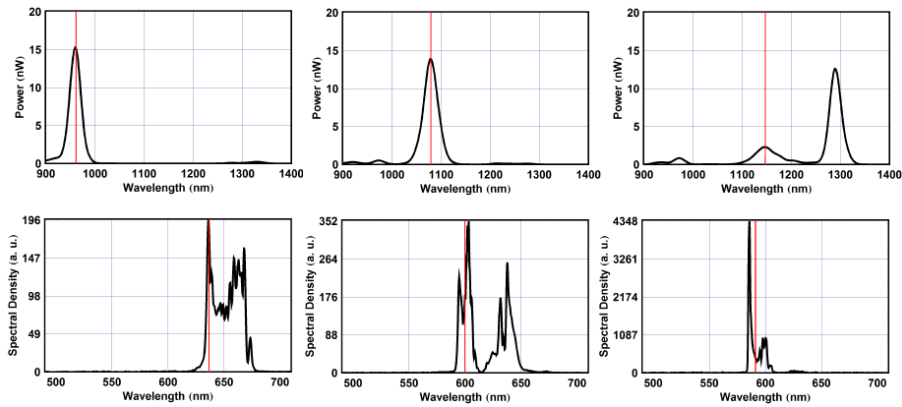


Fig. 4. Three spectra of the soliton (top) and the trapped light (bottom) as the launched pulse energy is increased (left: 21 pJ, center: 31 pJ, right: 40 pJ). Red lines mark the center wavelength of the soliton and a group velocity matched wavelength obtained from data in figure 2 [15].

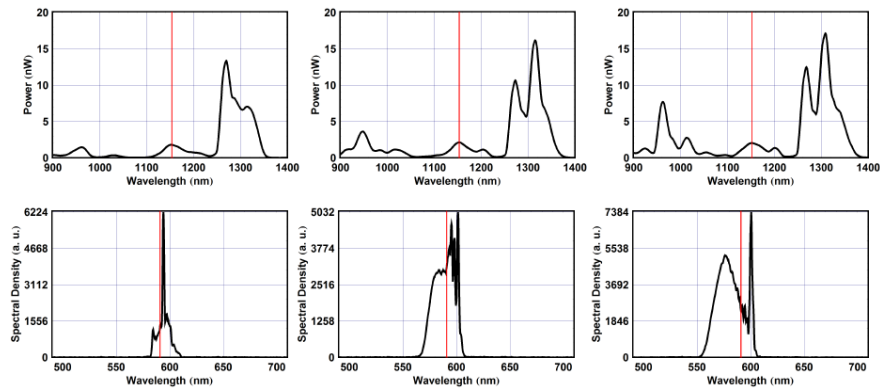


Fig. 5. Three spectra of the soliton (top) and the trapped light (bottom) for pulse energies exceeding those of figure 4 (left: 56 pJ, center: 88 pJ, right: 121 pJ). The Raman shift of the soliton is cancelled by Cherenkov radiation. The trapped light shifts almost completely beyond the wavelength that is group velocity matched to the soliton to shorter wavelengths and trails the soliton. Red line marks as in figure 4.

of Cherenkov radiation balances the stimulated Raman effect in the soliton and the soliton redshift terminates. Since the soliton energy is gradually being transferred to the Cherenkov radiation, the soliton decays [23]. Figure 5 also shows that nearly all of the trapped light shifts to wavelengths shorter than the group velocity matched wavelength. These are propagating slower than the soliton, that is the light escapes behind the soliton. Light at wavelengths travelling faster than the soliton collides with the soliton one last time and shifts to the blue beyond the group velocity matched wavelength. This is seen particularly clearly by examining the soliton and the trapped light in the time domain, which we describe next.

3.3. FROG and X-FROG measurements at low pulse energies

For low input pulse energies the soliton undergoes SSFS throughout the fiber and hence it is always slowing down. The ‘gravity-like’ part of the trap potential still exists at the fiber end. The trapped light is confined behind the barrier created by the soliton. In figure 6 second harmonic-FROG (SHG-FROG) measurements [16] of the visible part of the spectrum show the trapped pulse. All of the FROG and X-FROG traces in this paper use the same linear color scale shown. The trapped pulse has a duration of ~ 1 ps. The time-bandwidth product (FWHM) of this pulse is more than ten – the spectral width could support a sub 50-fs pulse.

The FROG retrieval requires a FROG grid as large as 2048x2048 pixels. Before retrieval, the wavelength is scaled by a factor to fit the data into a square grid [24]. After retrieval the wavelength is unscaled to recover the physical scale. The FROG error in figure 6 is 0.00468 (left column) and 0.00557 (right column). SHG-FROG has an ambiguity regarding the direction of time and the FROG measurement is not suitable to resolve the relative positions in time of the trapped pulse and soliton. Therefore we performed X-FROG measurements on the solitons and the trapped pulse by mixing the light from the fiber with the reference pulse (FWHM 35 fs) derived before the fiber and spectrally filtered. The X-FROG traces can be interpreted directly. Results are shown in figure 7, where the propagation direction is to the left. Again the ps-wide trapped pulse is measured. It is confined to the region behind the soliton. As the soliton redshifts and delays, the trapped light blueshifts to maintain group velocity matching with the soliton. Note that the trapped pulse trails the soliton by about 0.5 ps. This delay is due to the normal group velocity dispersion of the microscope objective used to collimate the light from the fiber. The measurements clearly show how the trapped pulse is strongly blocked by the soliton-induced barrier.

The retrieved pulse shapes in figure 6 (left) indicate that the trapped pulse has a small, low intensity shoulder on one side. The X-FROG measurements in figure 7 show that this shoulder extends behind the trapping soliton and reveal some ps temporal oscillations not resolved in the retrieved FROG traces. The shoulder seems induced by the asymmetry of the confining potential. The linearly increasing part of the trap potential caused by the SSFS is much more shallow than the sharp edge of the barrier.

The size of the trap can be estimated by equation 8. The soliton, when shifted to a wavelength around 1000 nm, maintains a near constant width of $T_0 = 60$ fs for different input pulse energies as measured separately by autocorrelation. With $T_R = 5$ fs [22] and a ratio $\beta_2/|\beta_{2,s}| \approx 1.5$ (see figure 2) this gives a trap length of 4 ps. The actual length of a pulse in this trap will be somewhat shorter as the pulse energy will not reach the height of the potential barrier of the trap due to tunneling. The observed pulse length of about 1 ps is in good agreement with this estimate.

3.4. Higher pulse energies and the end of trapping

When the input pulse energy in the fiber is sufficient for the soliton to reach the longer zero-dispersion wavelength, the behavior of the trapped light changes. SHG-FROG measurements of the trapped light are shown in figure 8. (FROG retrieval errors: 0.00449 (left), 0.00484 (right)).

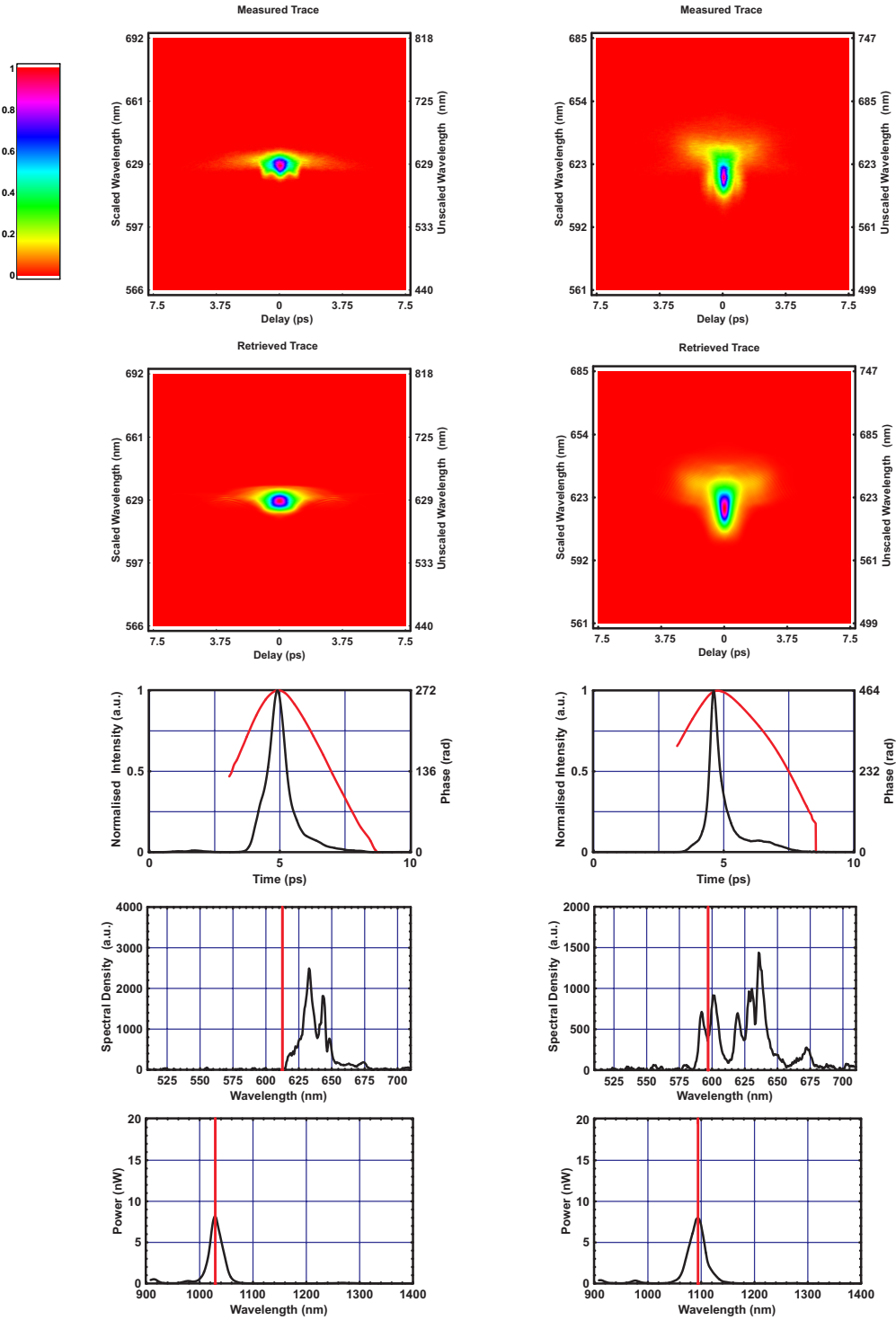


Fig. 6. Measured SHG-FROG traces (top row), retrieved traces (second row), and retrieved intensity and phase (third row) for the trapped light when the soliton is accelerating. Fourth and fifth row show the independently measured trapped pulse and soliton spectra, respectively. Pulse energies are: left: 26 pJ, right: 32 pJ. Explanation of FROG axes see text.

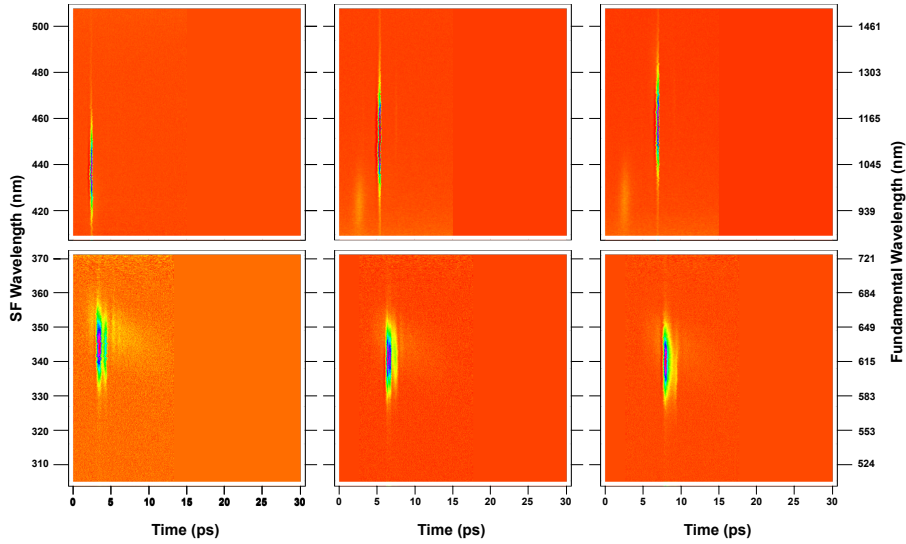


Fig. 7. X-FROG measurements of the soliton (top) and the corresponding trapped pulse (bottom) for low input pulse energies. The direction of propagation is to the left (pulse energies: left: 28 pJ, center: 34 pJ, right: 38 pJ). Increasing the energy redshifts (and therefore delays) the soliton. The trapped light is confined behind the soliton.

The pulse peak has widened considerably beyond 1 ps and the small shoulder of figure 6 has developed into a long tail. With more energetic input pulses the tail extends further.

This behavior again is a direct consequence of the soliton dynamics. When the soliton wavelength is stabilized by Cherenkov radiation, the acceleration terminates rapidly, but the soliton decays slowly [23]. The barrier part of the potential remains, but the gravity-like part disappears. Hence one side of the potential well vanishes and the light escapes the trap to one side creating the pronounced tail in figure 8. A higher launched pulse energy leads to a faster SSFS and the soliton acceleration turns off earlier on in the fiber. Thus the trapping ceases earlier and the trapped light can spread out more under dispersion during the remaining length of fiber. This is seen in figure 8 as the tail extends further for higher pulse energies.

Corresponding X-FROG traces of the trapped pulse and soliton after the soliton redshift has ceased are shown in figure 9. The soliton remains a barrier and prevents the trapped pulse from overtaking as before. On the other side the developing tail is clearly visible, extending more than 10 ps behind the soliton barrier (see also figure 8). Again the tail bears oscillations not resolved in the retrieved FROG traces. The shorter wavelengths in the tail travel slower due to the normal dispersion. The spectrum of the trapped pulse in figure 8 (right) is centered at 580 nm with a spectral width of 40 nm. At this wavelength the fiber dispersion is $\beta_2 \approx 45 \text{ ps}^2/\text{km}$ (figure 2). This leads to an expected length of the tail of about 10 ps per meter, in good agreement with the measured length. Thus as soon as the trapping terminates, the trapped light spreads quickly.

4. Yet higher pulse energies

By sacrificing the reference beam used in the X-FROG measurements we are able to further increase the pulse energy into the fiber. The soliton now reaches the wavelength stabilized by Cherenkov radiation even earlier in the fiber. Unfortunately, the large temporal width of the pulse and a small signal appearing at longer wavelengths made it impossible for our code to

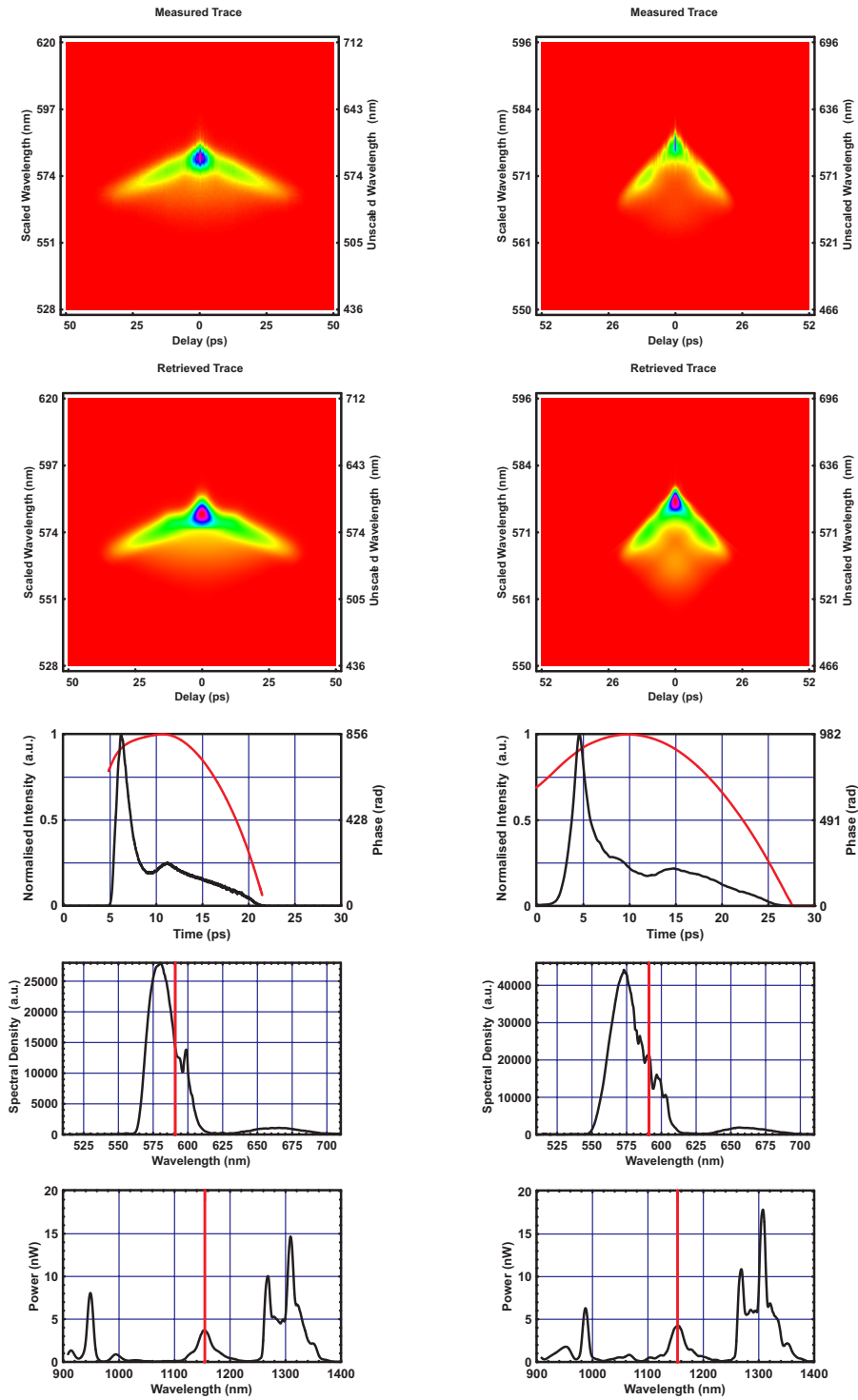


Fig. 8. Measured SHG-FROG traces (top row), retrieved traces (second row), and retrieved intensity and phase (third row) for the trapped light when the soliton has reached the second ZDW and acceleration is terminated (estimated energies: left: 125 pJ, right: 135 pJ). Rows four and five show the trapped pulse and soliton spectra, respectively. The trapped pulse has developed a long tail, which increases beyond the trap length as the trap is terminated earlier on in the fiber. Explanation of FROG axes see text.

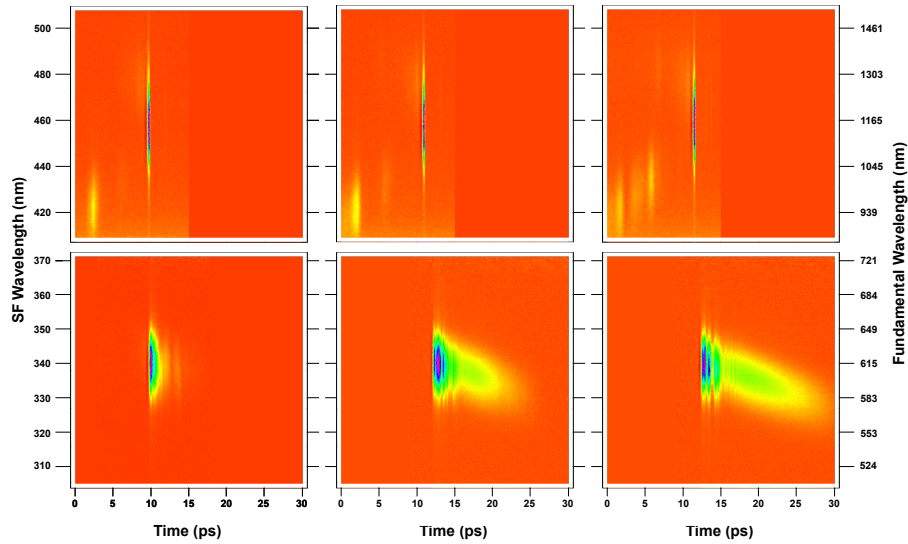


Fig. 9. X-FROG measurements of the soliton and the trapped pulse for higher input energies (est. energies: left: 39 pJ, center: 100 pJ, right: 120 pJ). The soliton shift is terminated by the Cherenkov effect. The trapped light escapes the trap behind the soliton. The barrier part of the potential is still present.

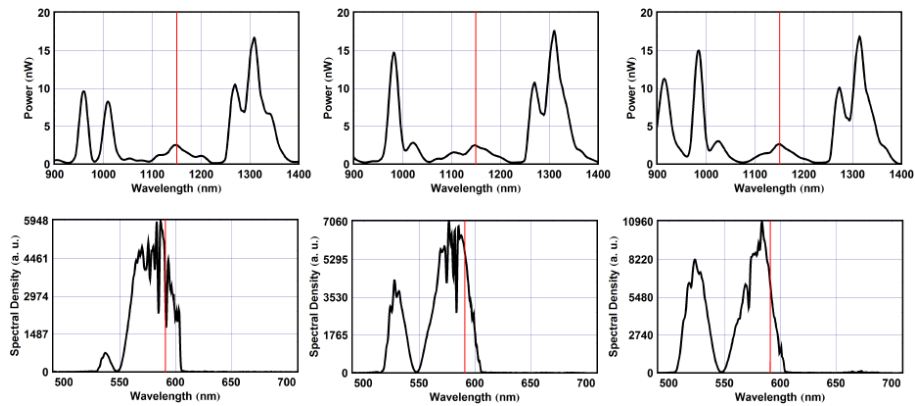


Fig. 10. The spectrum of the soliton (top) and the short-wavelength end of the supercontinuum (bottom) for pulse energies exceeding those of figure 5 (left: 170 pJ, center: 210 pJ, right: 280 pJ). The soliton reaches the longer ZDW even earlier in the fiber and multiple solitons undergo SSFS (top). The trapped light is released, but the spectrum extends further to the blue with a distinctive gap at 550 nm (bottom).

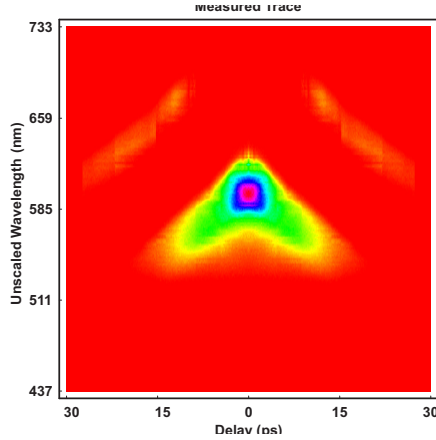


Fig. 11. SHG-FROG measurement of the trapped pulse for a pulse energy of 295 pJ corresponding to figure 10. The trace is similar to previous FROG measurements of the trapped light after the trapping has ended (see figure 8).

retrieve the FROG trace. The FROG trace is similar to traces of the trapped light at lower powers (compare to figure 8). The length of the tail is determined by the dispersion over the full fiber length. The wavelength of the pulse peak is arrested at ~ 590 nm. This stabilizes the trapped pulse and makes it independent of coupled input energy in this energy range.

The spectrum continues to reach shorter wavelengths, considerably below the group velocity-matched point (figure 10). We attribute the additional peak of light appearing below 550 nm to nonlinearly phase matched resonant wave mixing at the very input of the fiber [25, 17, 26]. This is consistent with the observation that the peak shifts to the blue with increasing energy. Similar behaviour has been seen in [19, 4]. In our case there is a particularly pronounced spectral gap at 550 nm, independent of input energy and of constant shape. In the infrared we see that multiple solitons, created from the input pulse by soliton fission, have shifted towards the long ZDW. The soliton that is arrested just short of the long ZDW is at a minimum of group velocity. The initially trapped light still trails the soliton and thus is of a wavelength shorter than the group velocity-matched wavelength. Light in the trap that had been propagating Δv faster than the soliton before release has undergone a spectral blueshift at the soliton to a group velocity Δv slower than the soliton [13].

5. Conclusion

By measurements in both the temporal and spectral domains, we show how the dynamics of a soliton determine both the wavelength and pulse-like nature of the short wavelength end of the supercontinuum. Light in the normal dispersion regime forms a trapped pulse governed by a potential consisting of a nonlinear barrier and a ‘gravity-like’ linear potential. The linear part is due to the SSFS which causes a negative acceleration of the soliton. As long as the soliton is accelerating, the trapping confines the light in time. When the SSFS terminates, the trapped light falls behind the soliton, moving to a wavelength associated with a group-velocity slower than the soliton. This effect dominates the shape of the supercontinuum at short wavelengths until resonant wave mixing with the input pulse further broadens the spectrum.

This setup allows for the creation and release of wavelength tunable picosecond pulses in the normal dispersion regime at any location along a microstructured fiber. The wavelength for the trapped pulse is obtained by choosing an appropriate dispersion profile of the fiber. The most

important parameter is the longer zero dispersion wavelength. If the fiber has a long ZDW that is longer than 1160 nm, then the SSFS would take the soliton further into the infrared before the acceleration terminates. The trapped pulse would shift to even shorter wavelengths and still be confined in time. Once the soliton is arrested, the trapped pulse has reached the final wavelength which is largely independent of pulse energy. Hence, the trapped pulse wavelength could be increased from this by use of lower input pulse energies or chirped input pulses.

6. Acknowledgements

We are indebted to Dmitry Skryabin, Andrey Gorbach, Scott Robertson, Franz Kärtner, Peter Staudt, Klaus Metzger and Wilson Sibbett for discussions and technical support. This work is supported by the EPSRC, the Royal Society, and the Leonhardt Group Aue.